CHAPTER 8

NUMERICAL SIMULATIONS OF THE ITCZ OVER THE INDIAN OCEAN AND INDONESIA DURING A NORMAL YEAR AND DURING AN ENSO YEAR

In this chapter, comparisons between the model-produced and analyzed streamlines, wind speeds, and rainfall from different horizontal resolutions are first presented and examined. The model performances are, furthermore, evaluated through the vertical profiles of the vertical velocity, specific humidity, and temperature, and through spatial distributions of mean kinetic energy and surface total heat flux. Finally, diurnal variations of rainfall, vertical velocity, and surface heat flux are investigated.

8.1 Indian Ocean

8.1.1 Streamlines and Wind Speeds

Figures 8.1a-d and 8.2a-d show the analyzed and day-1 simulated streamlines and wind speeds for 00 UTC 30 January 1997 obtained from the NRL/NCSU model and the PSU-NCAR MM5, respectively. In general, both models can simulate the low-level westerly convergence (with amplitude 2-8 ms^{-1}) over the southern Indian Ocean quite reasonably. Meanwhile, since the location of a cyclonic eddy at 2.5°N is not accurately placed by both models, the simulated wind flows in the western Indian Ocean are quite different from the analysis. The effect of different model resolutions is clearly seen in the NRL/NCSU model's simulations (Figs. 8.1a-d). The FGM grid size results in overall highest wind speeds. In contrast, the grid resolution has little effect in simulations from

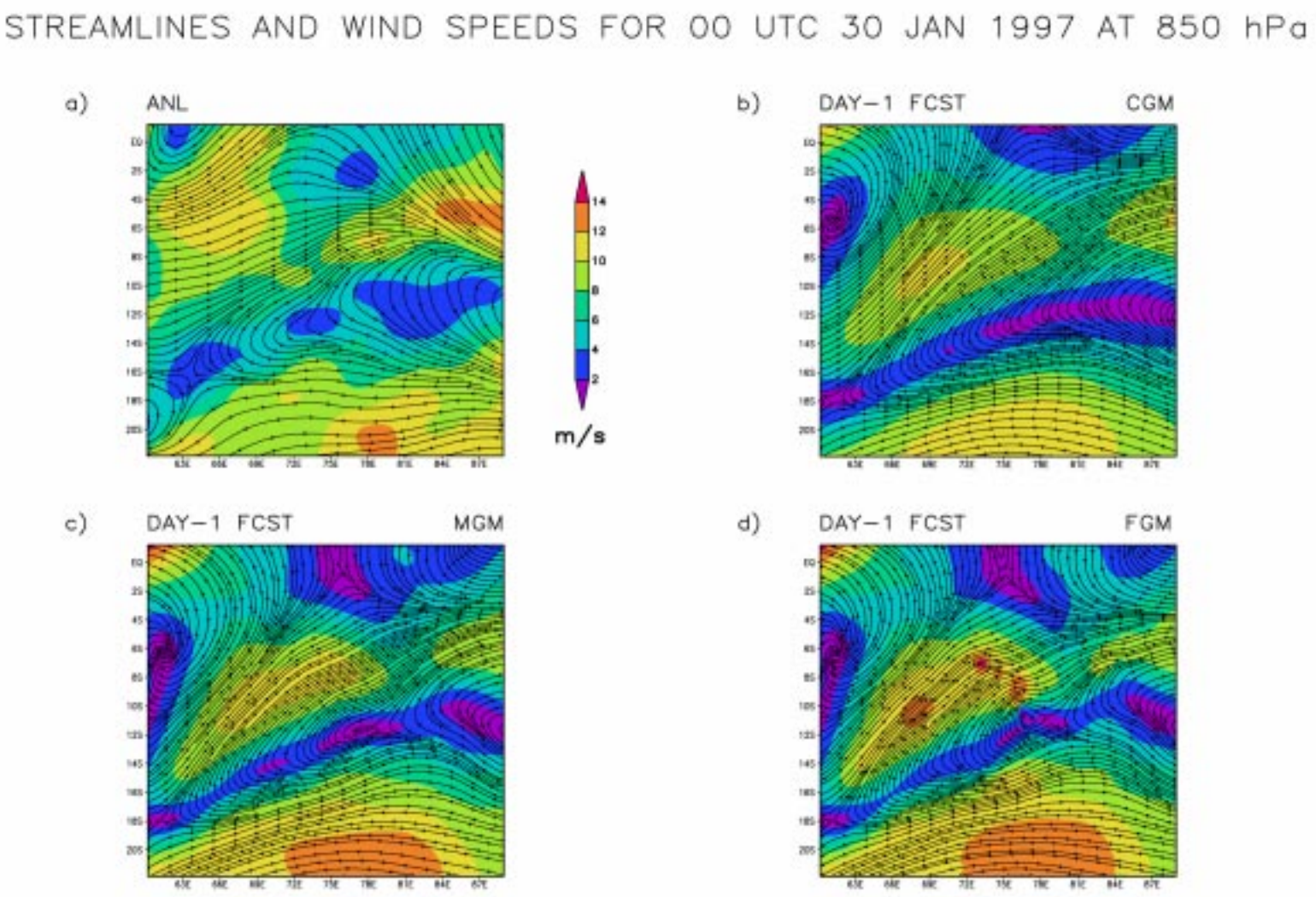

Figure 8.1. a) The analyzed and day-1 simulated streamlines and wind speeds for 00 UTC 30 January 1997 at 850 hPa in b) CGM, c) MGM, and d) FGM grid resolutions for the Indian Ocean case from the NRL/NCSU model.

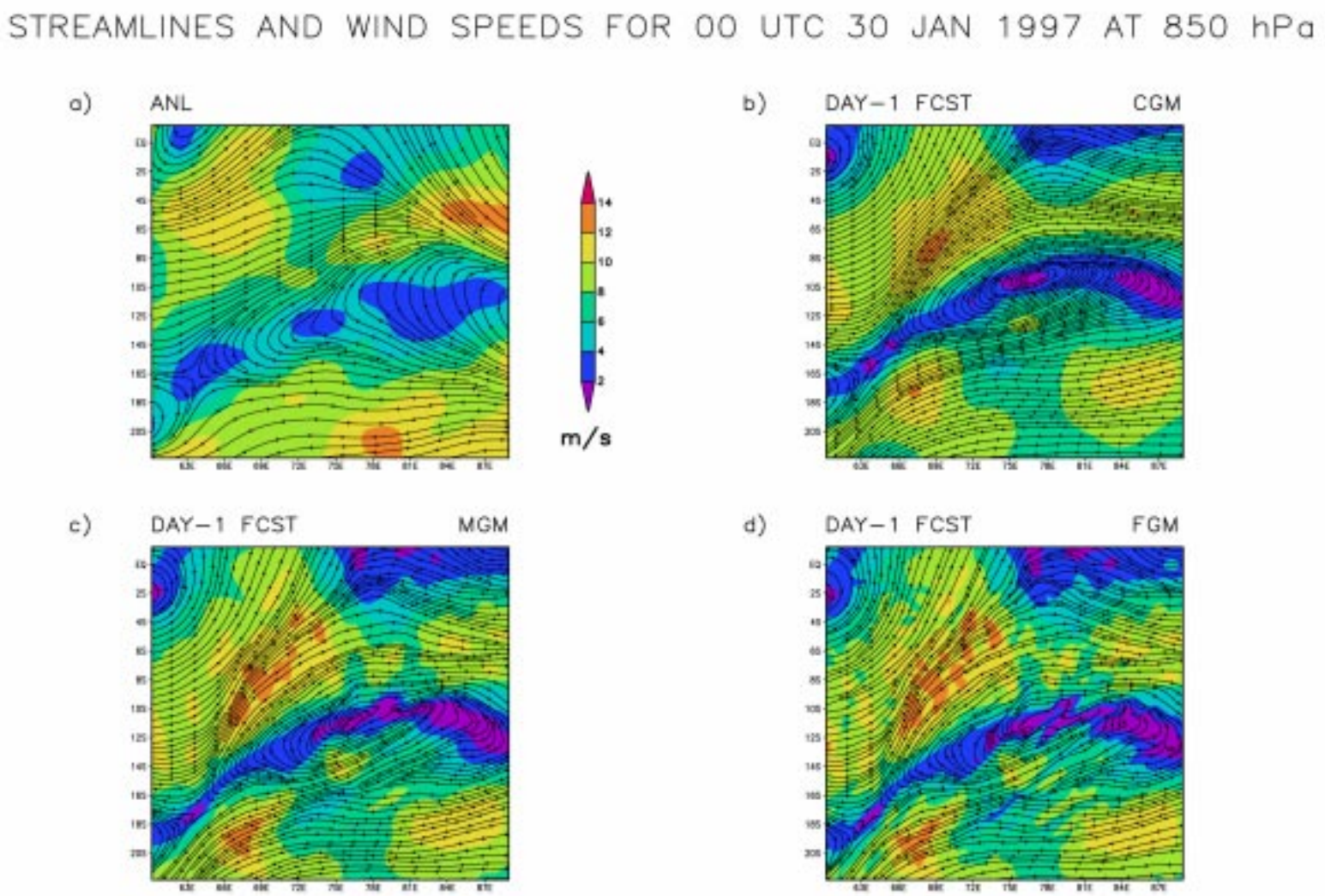

Figure 8.2. As in Fig. 8.1, except from the PSU-NCAR MM5.

the PSU-NCAR MM5 (Figs. 8.2a-d). The forecast skills given for the FGM resolution (Table 8.1) show that the NRL/NCSU model results in higher average error (RMSE) for U component, but smaller for V component than the PSU-NCAR MM5. Generally, higher correlation (CORR) for U component is given by the PSU-NCAR MM5, and for V component by the NRL/NCSU model.

At 00 UTC 31 January 1997, the westerly winds become stronger (with amplitudes of 8-14 ms^{-1}) indicating active period of monsoon. The NRL/NCSU model fails to simulate the convergent westerly winds over the southern Indian Ocean (Figs. 8.3a-d). Instead, the model tends to produce easterly winds with an amplitude between 6 and 14 ms^{-1} reflecting high BIAS and RMSE values. Additionally, cyclonic eddies at (18°S; 62°E) and (13°S; 88°E) are missing from the simulations. Similarly, the PSU-NCAR MM5 does not accurately capture the westerly wind convergence (Figs. 8.4a-d). Moreover, the wind speeds are generally underestimated with an RMSE value of 4.4 ms^{-1}. These results indicate inability of the models to generate and maintain the low-level westerly winds during the active monsoon up to 48 hours of integration.

The errors in these model simulations of the monsoon circulation could be due to a number of factors. One of the main factors is deficiency in tropical diabatic heating in the model. In the tropics, the constraint of geostrophy on the divergent circulation is weak so there is considerable sensitive to the diabatic heating field, particularly that associated with moist processes. The vertical motion and moisture fields and hence diabatic heat sources are generally ill defined in the initial analysis and causing model spin up problem. This could result in heat sources developing at incorrect locations and times.

Table 8.1. Forecast skill statistics for the Indian Ocean case.

Date	Var.	Mean (ms^{-1})			BIAS (ms^{-1})		RMSE (ms^{-1})		CORR	
		ANL	NCSU	MM5	NCSU	MM5	NCSU	MM5	NCSU	MM5
00 UTC 30 Jan 97	U	-0.1	-0.2	1.3	-0.1	1.4	5.7	4.6	0.70	0.82
	V	0.5	2.0	1.4	1.4	0.9	3.2	4.4	0.59	0.22
00 UTC 31 Jan 97	U	-0.4	-9.1	-0.3	-8.7	0.2	9.9	5.5	0.82	0.74
	V	-1.3	-3.0	-2.0	-1.6	-0.7	3.9	4.4	0.37	0.10
00 UTC 30 Jan 98	U	-5.5	-8.3	-4.6	-2.8	0.9	4.1	2.4	0.16	0.31
	V	0.3	-0.3	1.7	-0.6	1.4	1.8	3.2	0.74	0.02
00 UTC 31 Jan 98	U	-5.9	-11.5	-4.3	-5.6	1.6	6.3	2.8	0.09	0.29
	V	0.9	-2.4	-1.4	-3.3	-2.3	4.2	4.2	0.36	-0.24

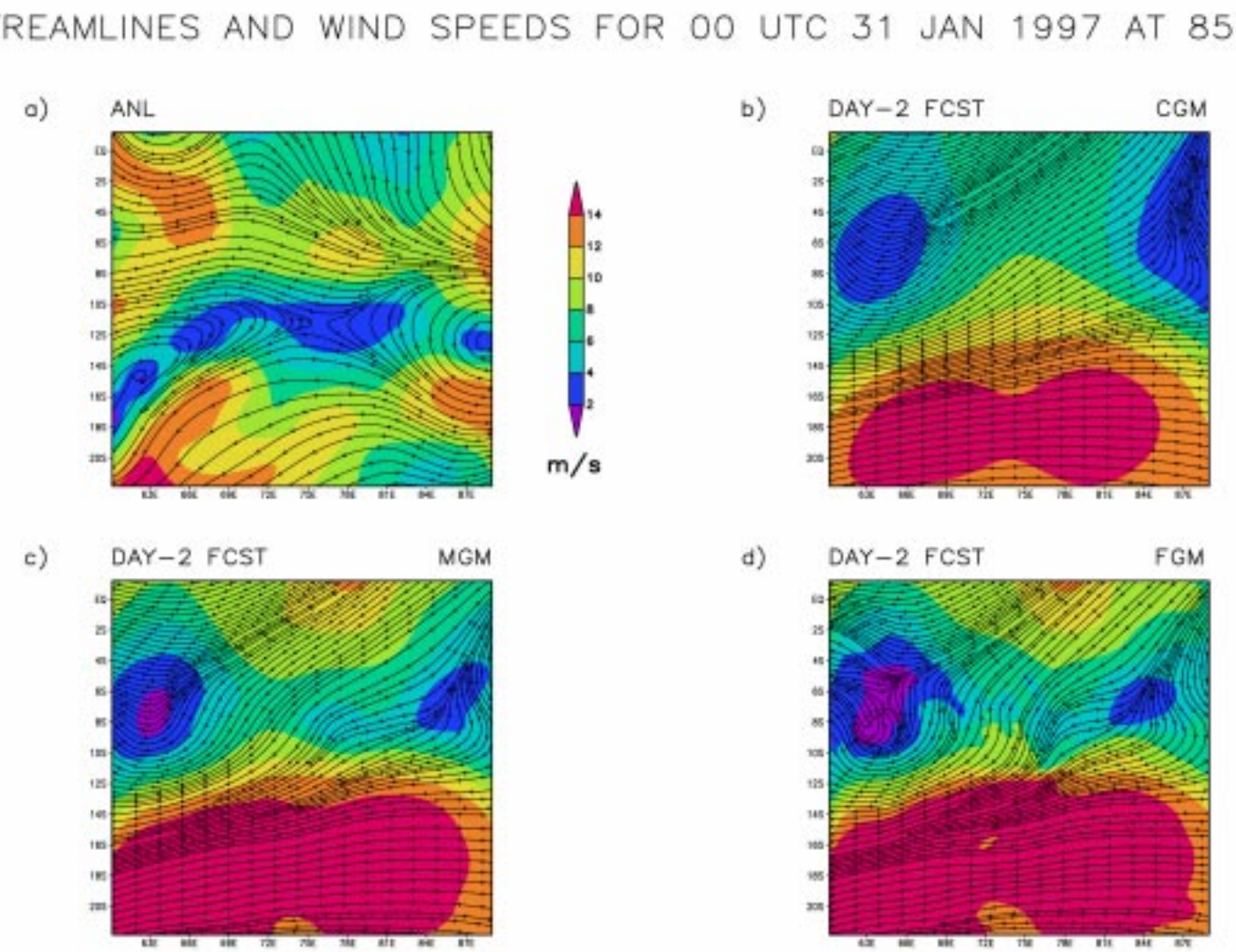

Figure 8.3. a) The analyzed and day-2 simulated streamlines and wind speeds for 00 UTC 31 January 1997 at 850 hPa in b) CGM, c) MGM, and d) FGM grid resolutions for the Indian Ocean case from the NRL/NCSU model.

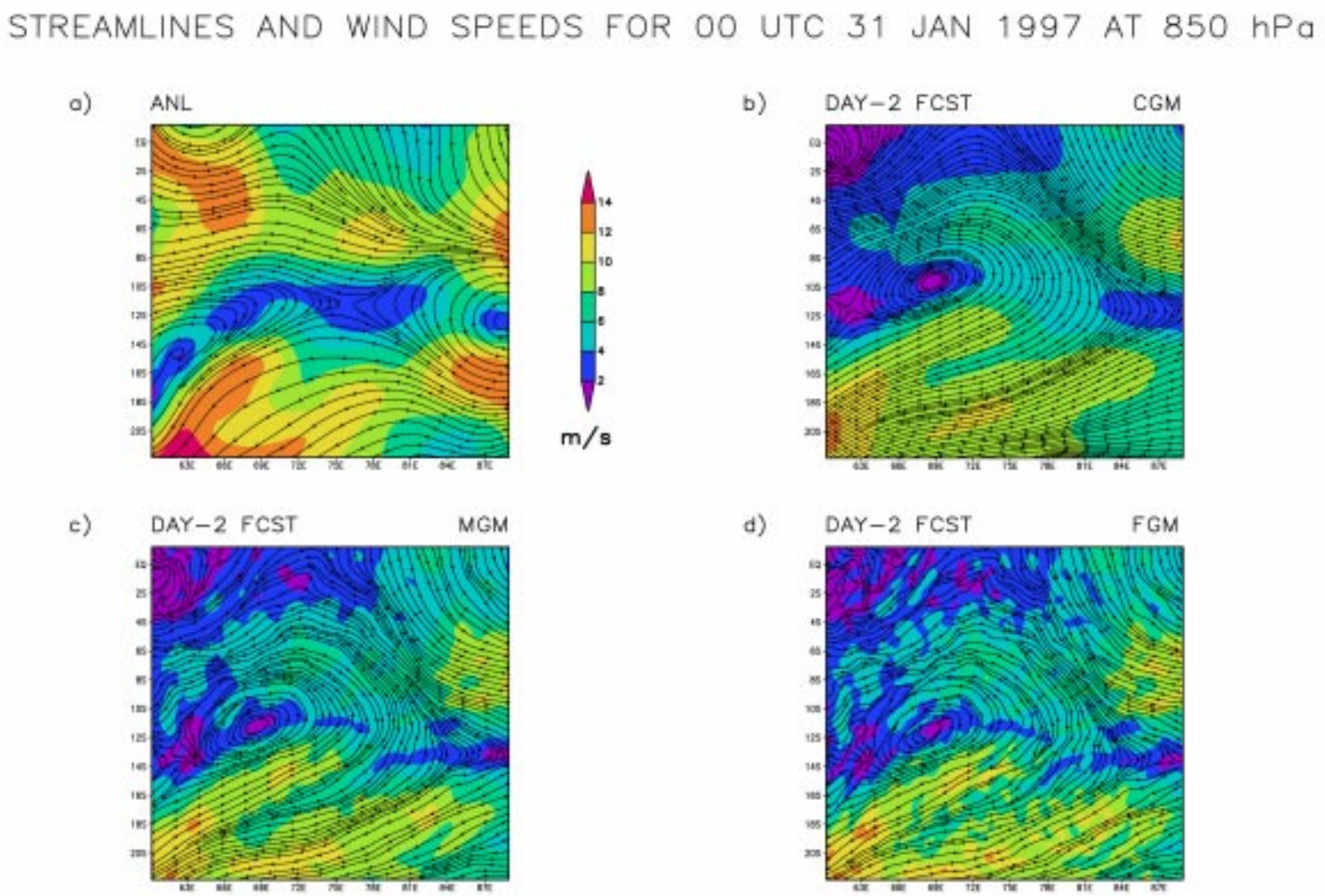

Figure 8.4. As in Fig. 8.3, except from the PSU-NCAR MM5.

Figures 8.5a-d and 8.6a-d show the analyzed and day-1 simulated streamlines and wind speeds for 00 UTC 30 January 1998 obtained from the NRL/NCSU model and the PSU-NCAR MM5. The NRL/NCSU model can produce a realistic response of the easterly winds due to anomalous warm SSTs over the western Indian Ocean (Figs. 8.5a-d), even though the overall wind speeds are slightly overestimated. Therefore, the CORR values for U and V components are 0.16 and 0.74. Similarly, the PSU-NCAR MM5 can simulate the easterly winds and wind speeds quite reasonable (Figs. 8.6a-d). Since the easterly convergence over the western Indian Ocean are not accurately placed, the CORR values for U and V components are 0.31 and 0.02, respectively.

At 00 UTC 31 January 1998, the NRL/NCSU model can still produce the easterly winds (Figs. 8.7a-d). However, the position of simulated convergent winds over the western Indian Ocean is displaced to the south. Moreover, higher wind speeds for both U and V components result in low CORR values (0.09 and 0.36). Similar results are found in the PSU-NCAR MM5 simulations (Figs. 8.8a-d). Although the overall wind speeds can be simulated reasonably well, the CORR values for U and V components are 0.29 and -0.24.

8.1.2 Rainfall

Figures 8.9a-d and 8.10a-d show the OLR distribution and day-1 simulated accumulated rainfall for 00 UTC 31 January 1997 obtained from the NRL/NCSU model and the PSU-NCAR MM5, respectively. Overall, both models can capture the maximum rainfall over the eastern Indian Ocean consistent with low values of the OLR data (The daily OLR values $\leq$ 200 Wm^{-2} indicate deep convection). A considerable increase in maximum

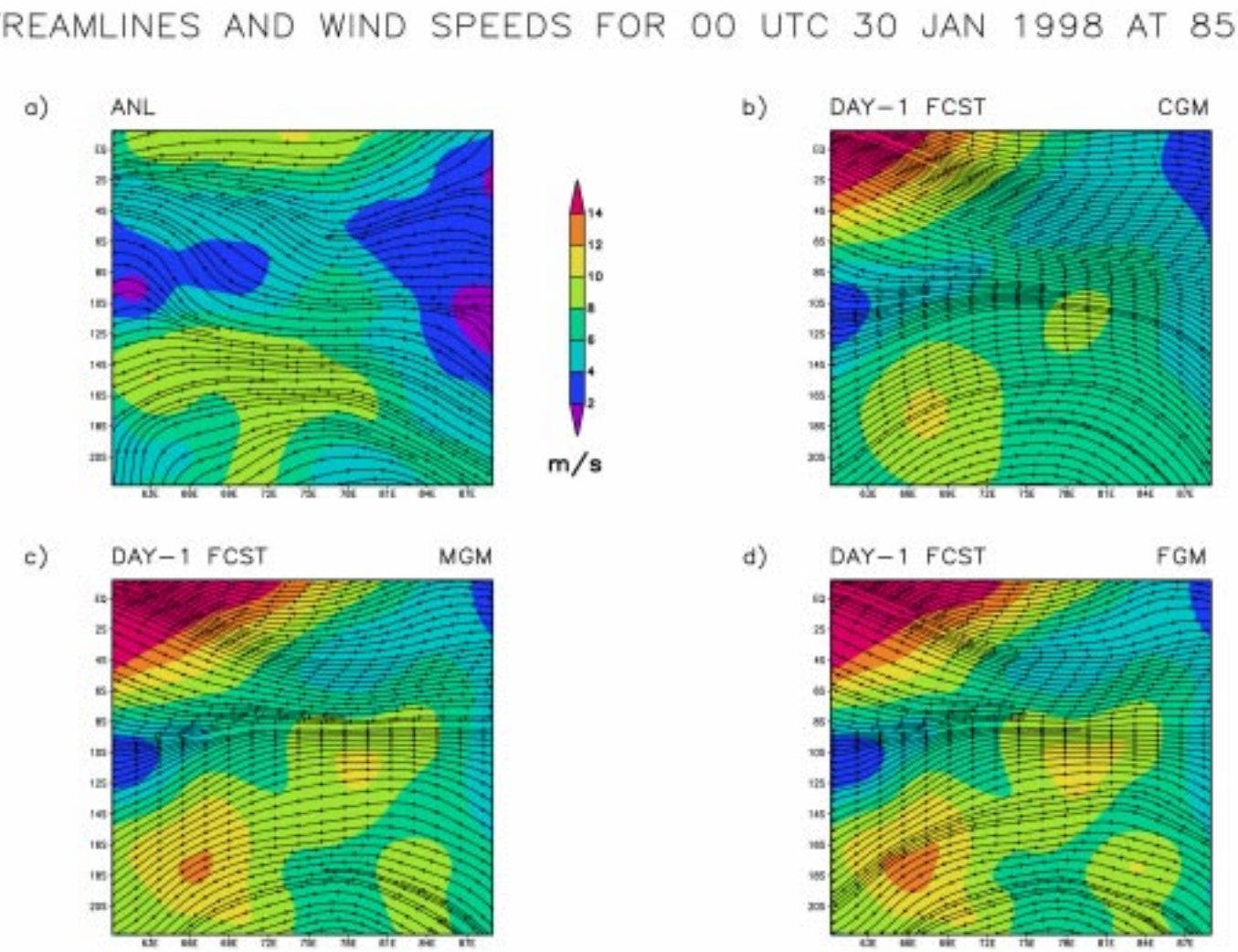

Figure 8.5. a) The analyzed and day-1 simulated streamlines and wind speeds for 00 UTC 30 January 1998 at 850 hPa in b) CGM, c) MGM, and d) FGM grid resolutions for the Indian Ocean case from the NRL/NCSU model.

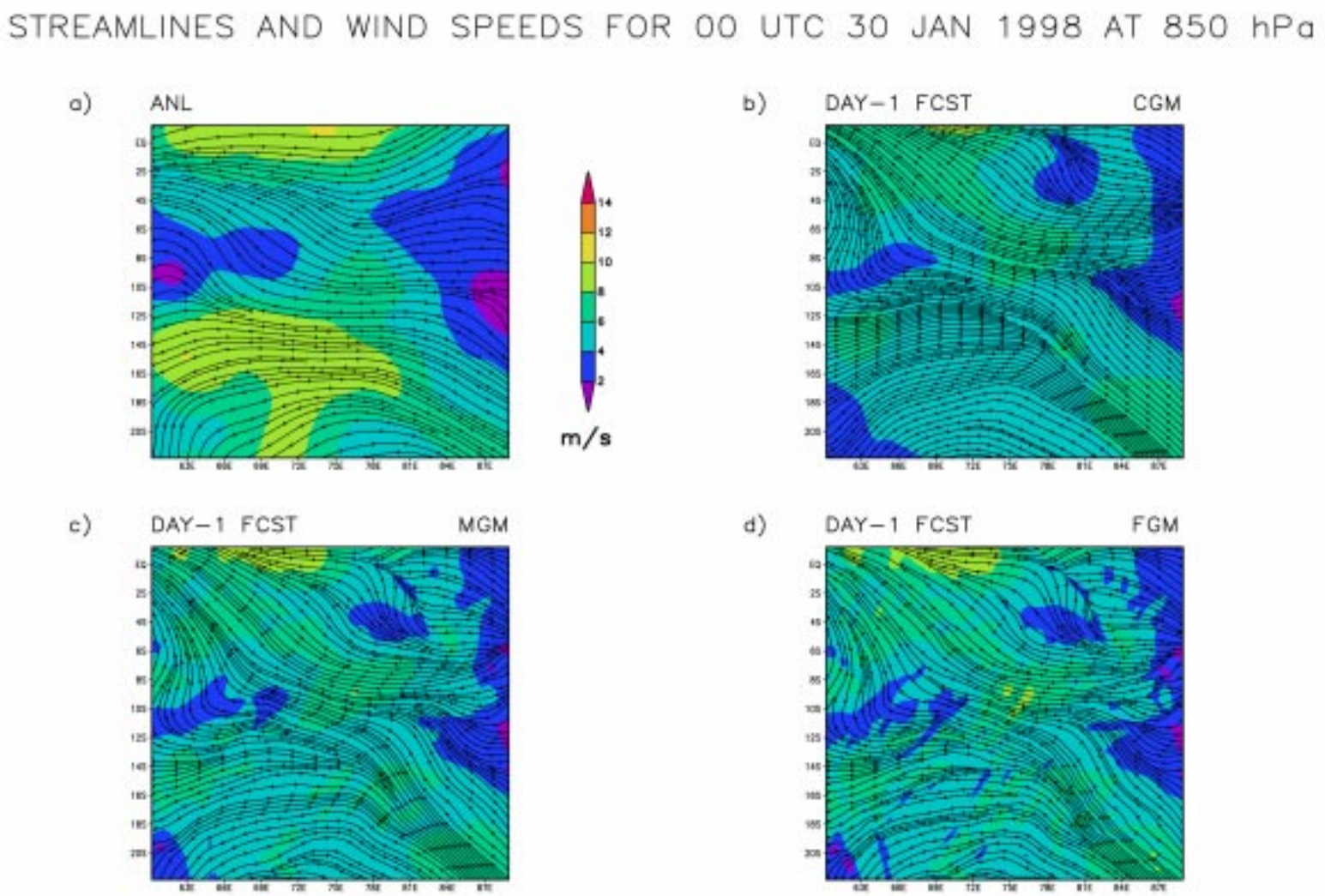

Figure 8.6. As in Fig. 8.5, except from the PSU-NCAR MM5.

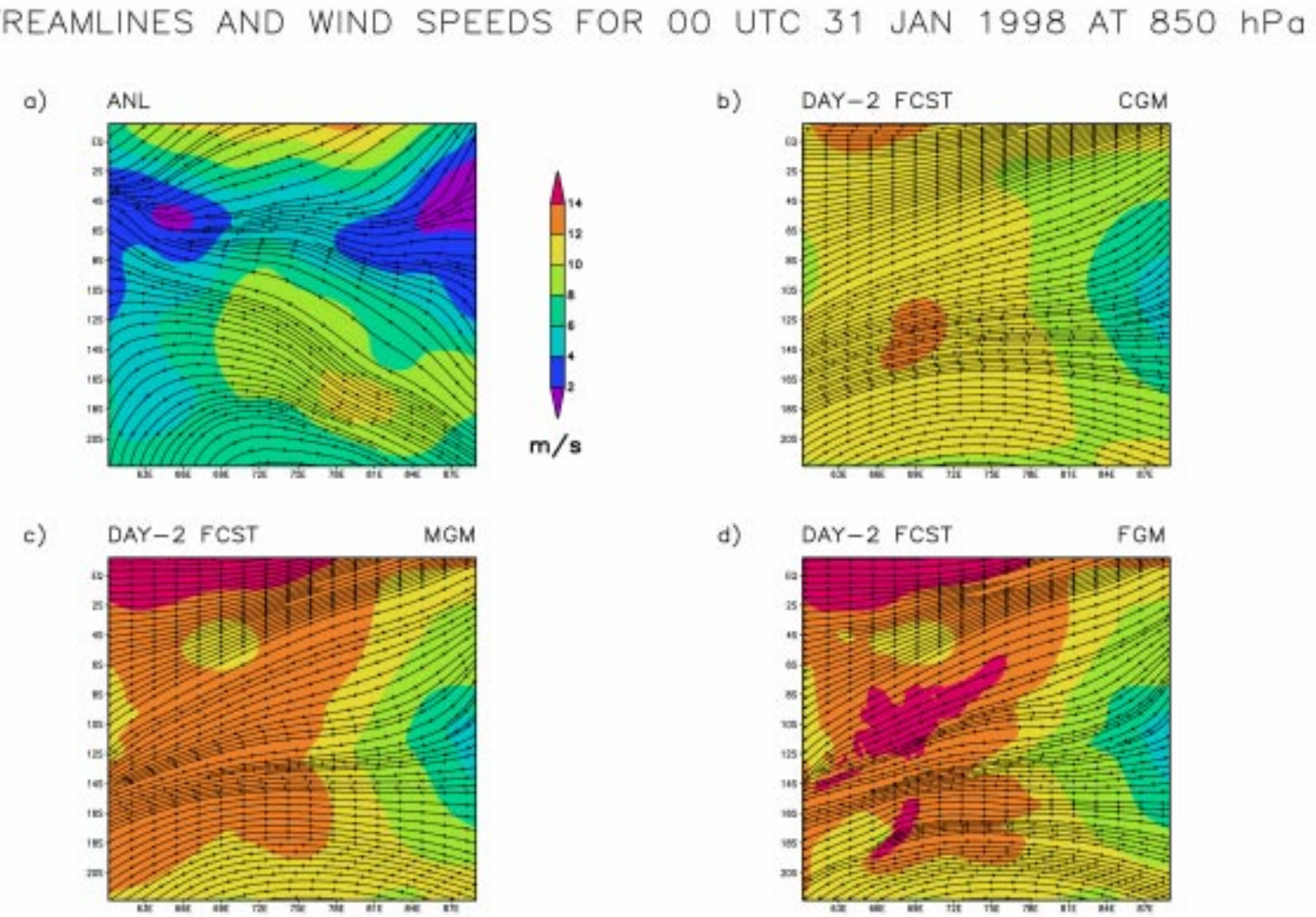

Figure 8.7. a) The analyzed and day-2 simulated streamlines and wind speeds for 00 UTC 31 January 1998 at 850 hPa in b) CGM, c) MGM, and d) FGM grid resolutions for the Indian Ocean case from the NRL/NCSU model.

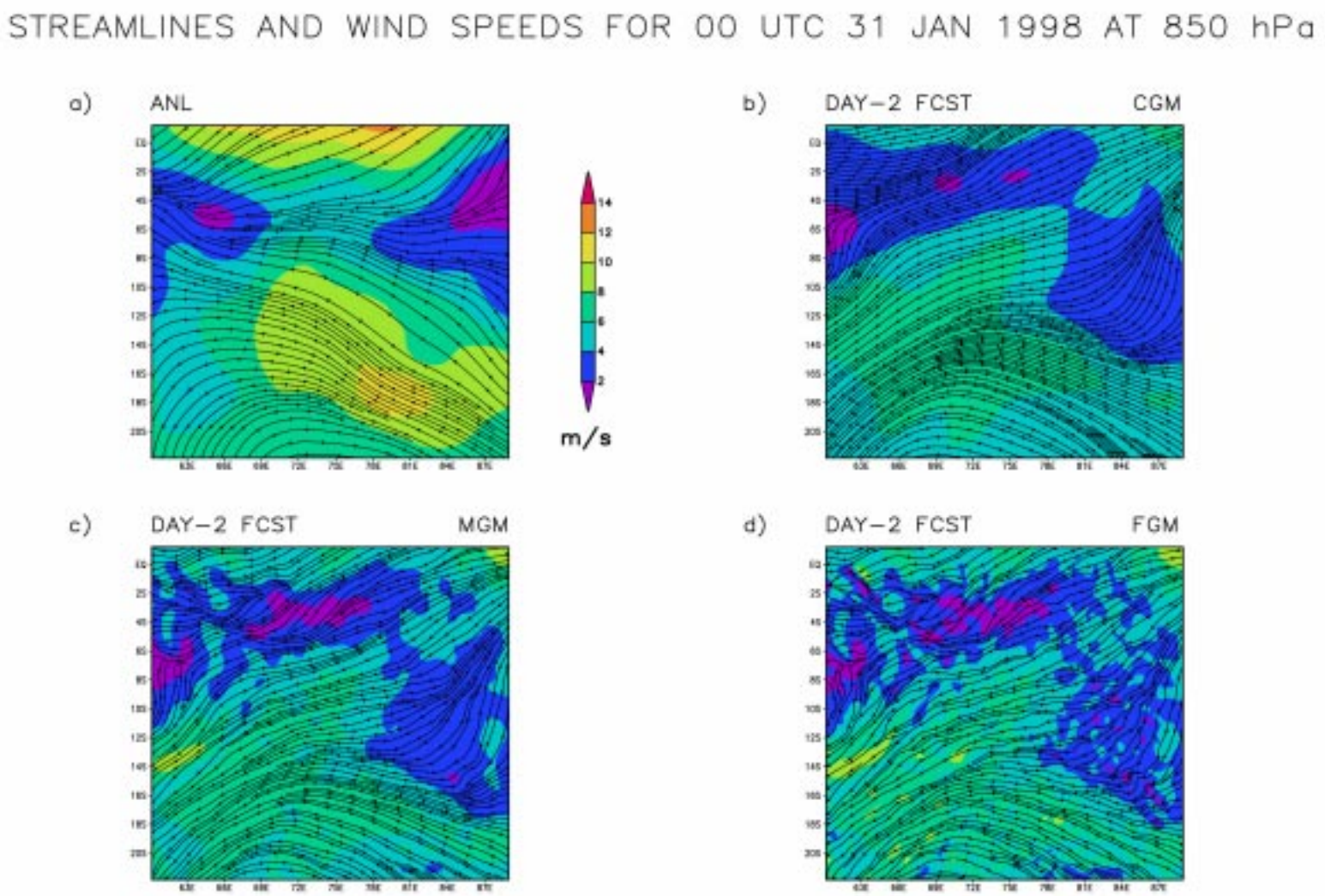

Figure 8.8. As in Fig. 8.7, except from the PSU-NCAR MM5.

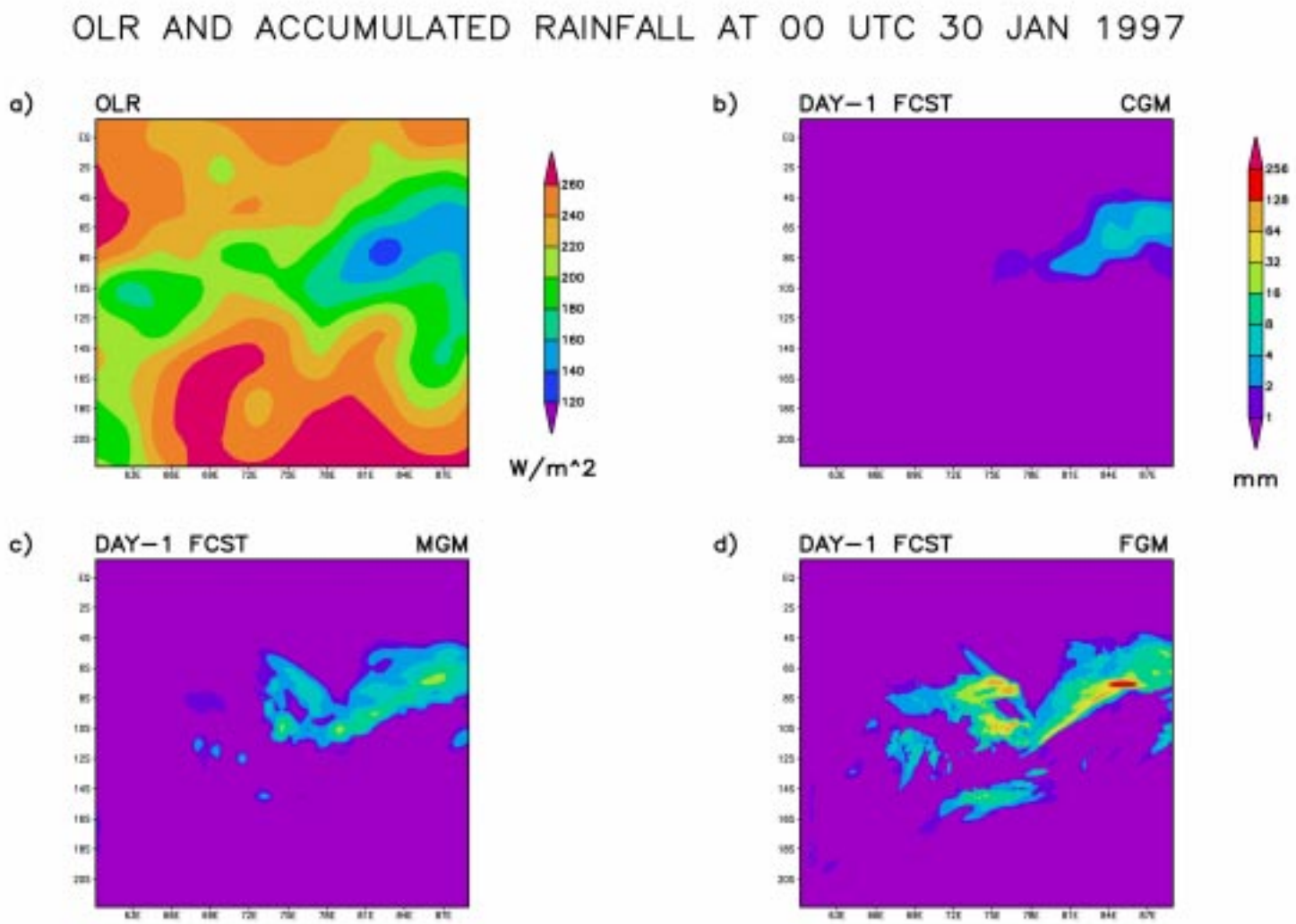

Figure 8.9. a) The OLR distribution and day-1 simulated accumulated rainfall ending at 00 UTC 30 January 1997 in b) CGM, c) MGM, and d) FGM grid resolutions for the Indian Ocean case from the NRL/NCSU model.

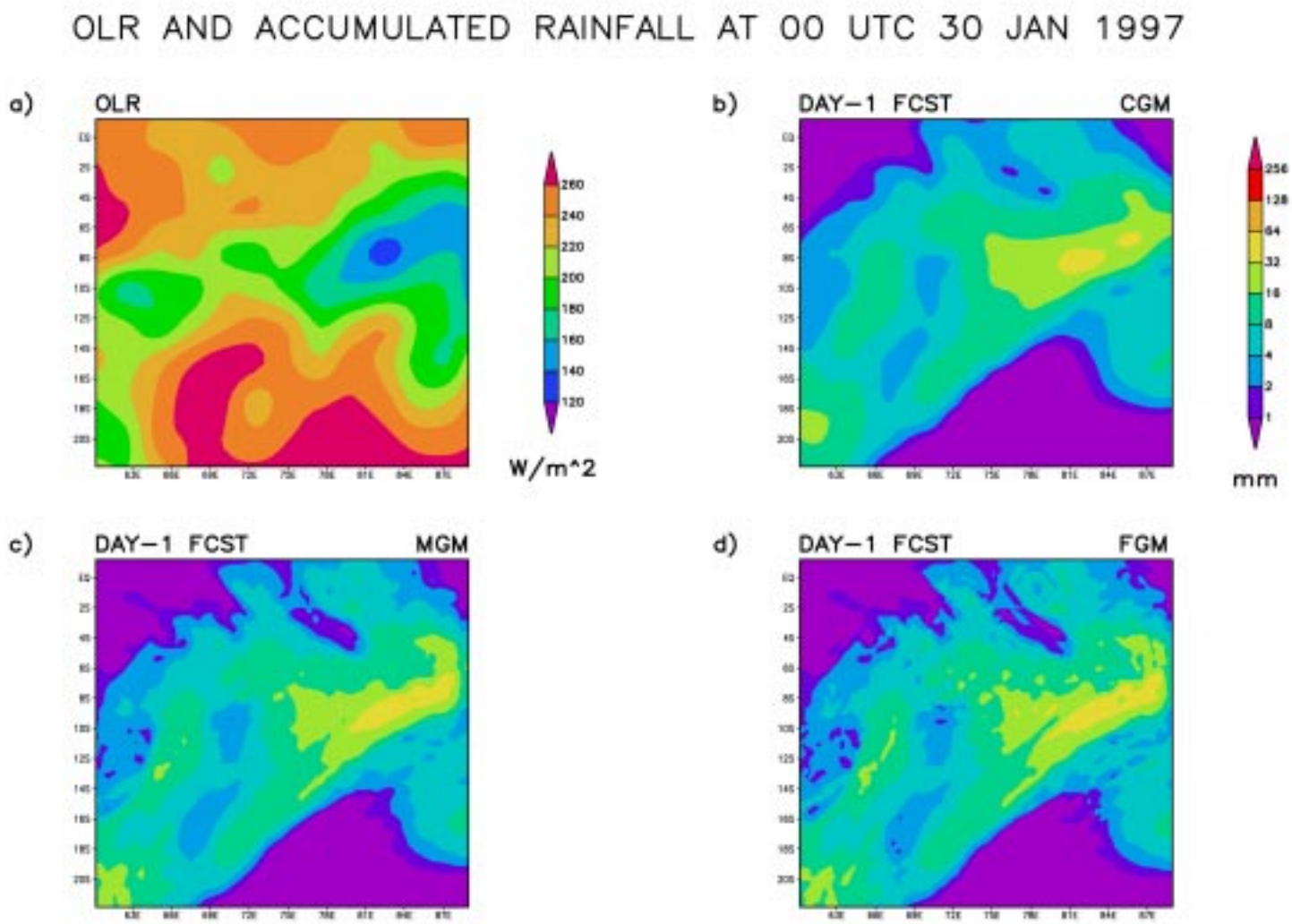

Figure 8.10. As in Fig. 8.9, except from the PSU-NCAR MM5.

rainfall is simulated by the NRL/NCSU model as the model's resolution increased (Figs. 8.9a-d), i. e., 8 mm day^{-1} for the CGM resolution to 200 mm day^{-1} for the FGM resolution. Additionally, an increase in the area of rainfall is also found as the model's resolution is increased. On the other hand, little improvement in maximum rainfall amongst different resolutions exists for the PSU-NCAR MM5 simulations (Figs. 8.10a-d). Moreover, rainfall distributions cover a broad rain band structure which might not be realistic. A number of factors could be responsible for this major deficiency in the model. An obvious factor is deficiencies in physical parameterizations, particularly boundary layer formulation and surface processes.

For day-2 of model integration at 00 UTC 31 January 1997, the heaviest rainfall (10 mm day^{-1} for the CGM and 200 mm day^{-1} for the FGM resolutions) is still captured by the NRL/NCSU model in the eastern Indian Ocean and is in good agreement with low OLR values (Figs. 8.11a-d). Although the low-level winds are not simulated well at this time, there is definitely an improvement in the rainfall simulation. The differences in the area of rainfall again exist for different resolutions. In contrast, the PSU-NCAR MM5 simulates much smaller rainfall rates (a maximum of 40 mm day^{-1} in the FGM resolution) during this time (Figs. 8.12a-d). Rainfall covers almost the domain, which is not really consistent with the OLR data.

Figures 8.13a-d and 8.14a-d show the OLR distribution and day-1 simulated accumulated rainfall for 00 UTC 30 January 1998 obtained from the NRL/NCSU model and the PSU-NCAR MM5, respectively. It is clear from these figures that overall rainfall magnitudes are much smaller than those at 00 UTC 30 January 1997. The NRL/NCSU model captures only a small extent of rain with a maximum of 10 mm day^{-1} in the FGM

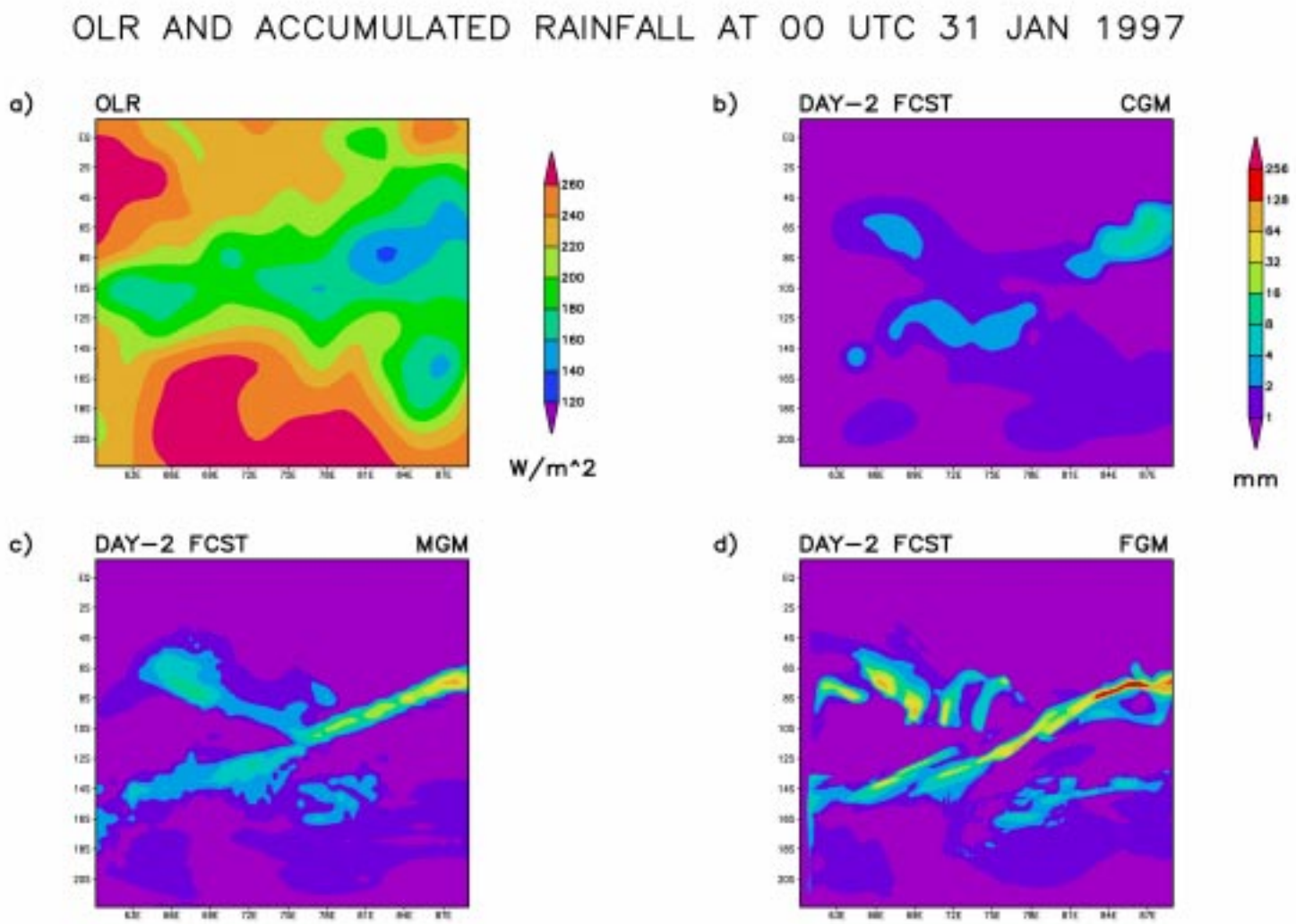

Figure 8.11. a) The OLR distribution and day-2 simulated accumulated rainfall ending at 00 UTC 31 January 1997 in b) CGM, c) MGM, and d) FGM grid resolutions for the Indian Ocean case from the NRL/NCSU model.

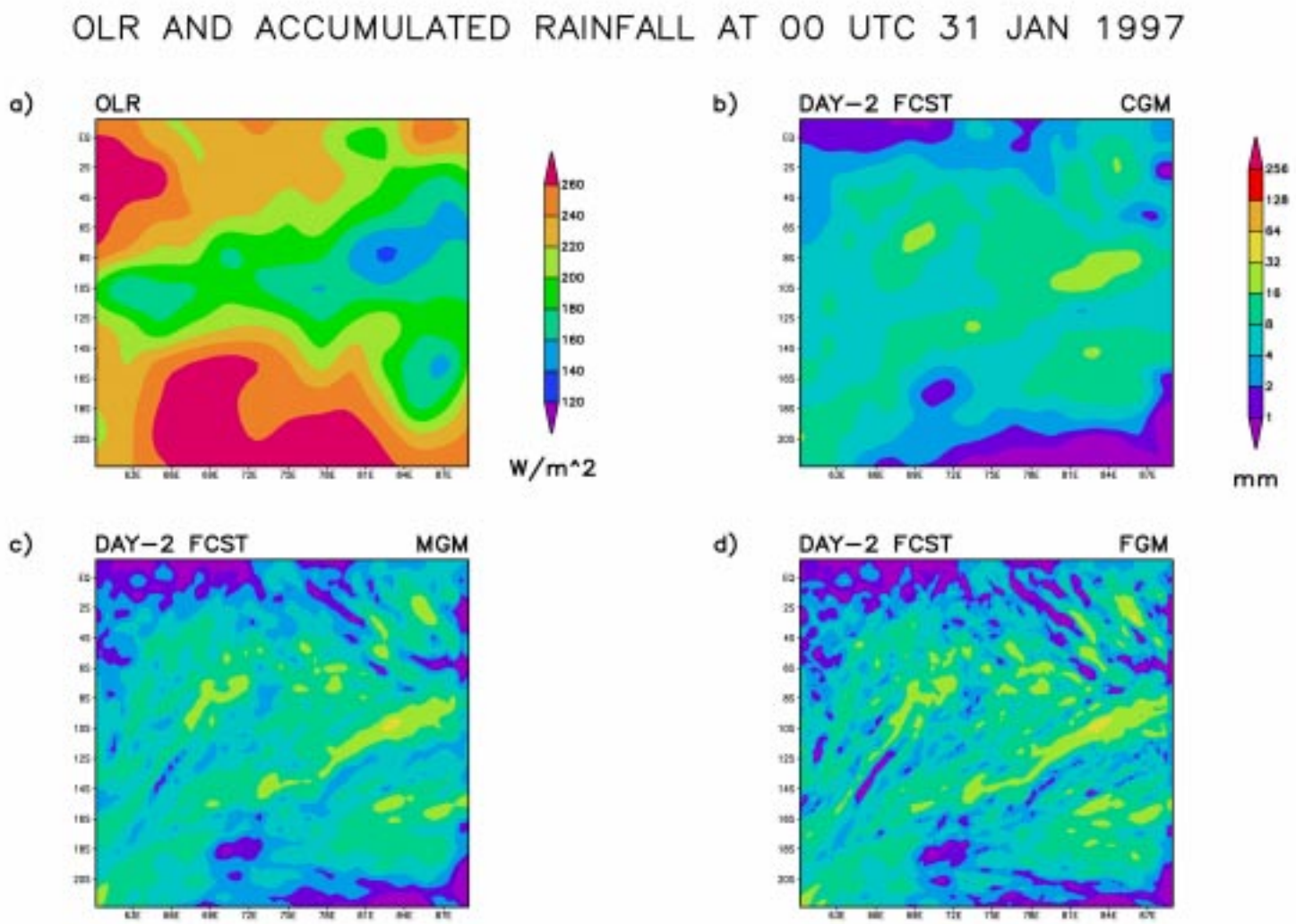

Figure 8.12. As in Fig. 8.11, except from the PSU-NCAR MM5.

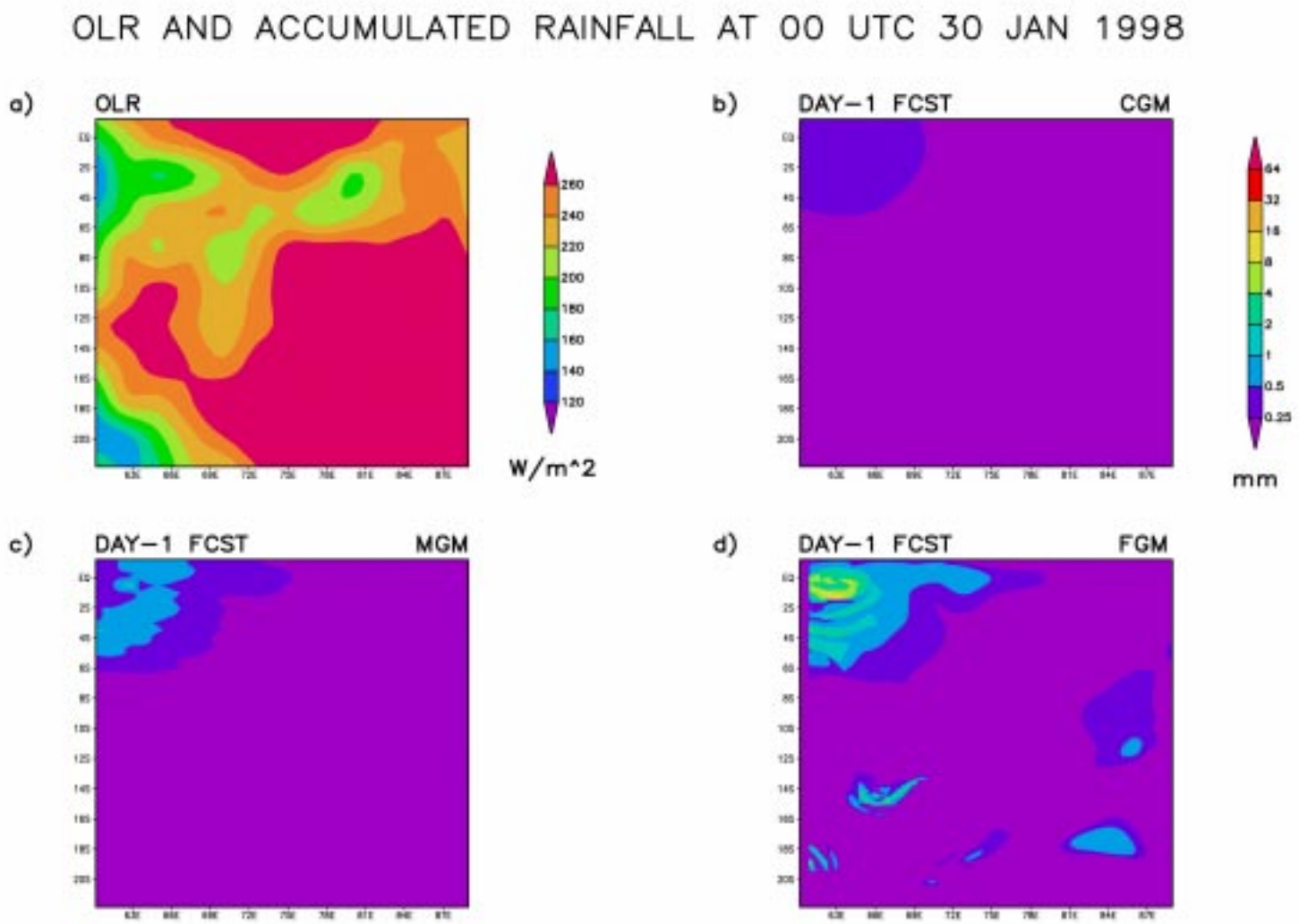

Figure 8.13. a) The OLR distribution and day-1 simulated accumulated rainfall ending at 00 UTC 30 January 1998 in b) CGM, c) MGM, and d) FGM grid resolutions for the Indian Ocean case from the NRL/NCSU model.

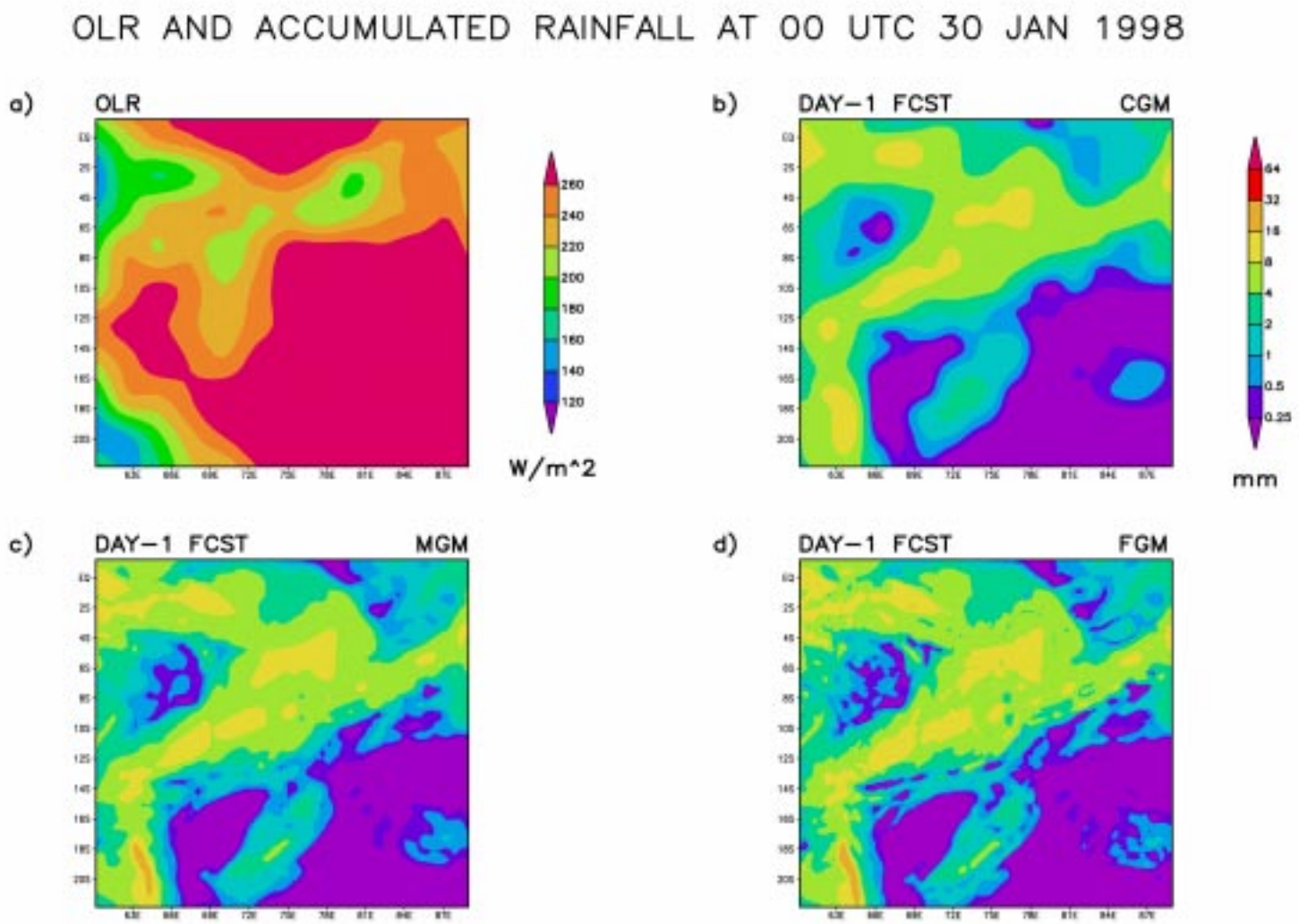

Figure 8.14. As in Fig. 8.13, except from the PSU-NCAR MM5.

resolution over the equatorial western Indian Ocean (Figs. 8.13a-d). Enhanced rainfall in this region is mainly attributed to anomalous warmer SSTs. Due to strong subsidence over the central and eastern Indian oceans, deep convection is not present in these regions. The PSU-NCAR MM5, on the other hand, simulates rainfall with a maximum of 20 mm day^{-1} over the southwestern Indian Ocean which is consistent with the lowest OLR values (Figs 8.14a-d). However, rainfall covers the western and central Indian oceans.

At 00 UTC 31 January 1998, the deep convection as inferred from OLR moves slightly to the east. This is in close agreement with the rainfall distributions simulated by the NRL/NCSU model (Figs. 8.15a-d), although a maximum rainfall of 50 mm day^{-1} occurs to the south of the convection. In contrast, the location of higher rainfall rates simulated by PSU-NCAR MM5 is almost the same as that at 00 UTC 30 January 1998 (Figs. 8.16a-d). At this time, the magnitude of maximum rainfall increases to about 50 mm day^{-1}.

8.1.3 Zonal Vertical Cross Section of Vertical Velocity, Specific Humidity, and Temperature

This section presents the model's response of the vertical cross section of the simulated vertical velocity given by $\omega = dp/dt$, specific humidity, and temperature obtained from the NRL/NCSU model. All results are presented as the meridional average between 0° and 15°S from the FGM resolution. The specific humidity and temperature profiles are given as the difference between the model simulation and the analysis.

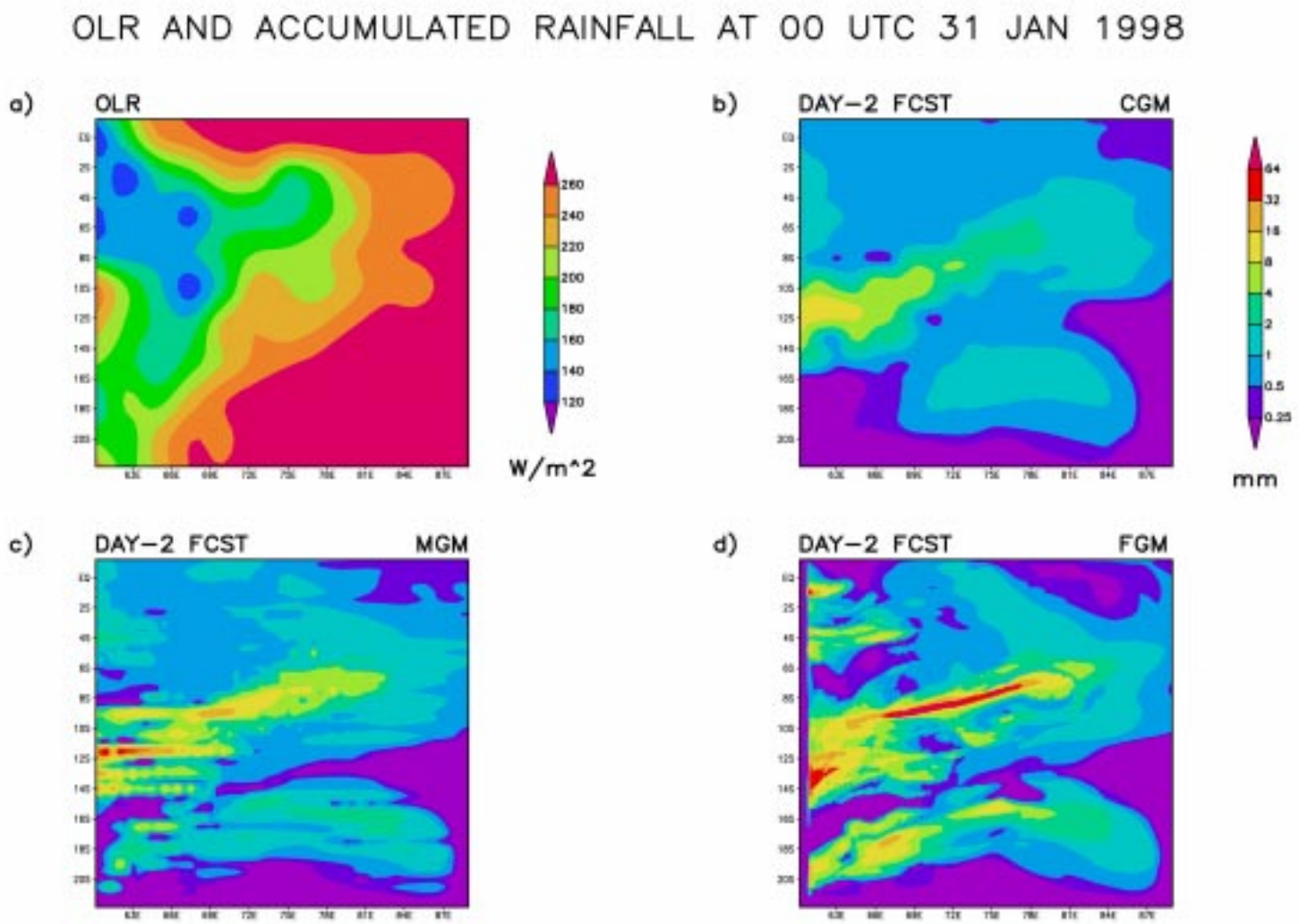

Figure 8.15. a) The OLR distribution and day-2 simulated accumulated rainfall ending at 00 UTC 31 January 1998 in b) CGM, c) MGM, and d) FGM grid resolutions for the Indian Ocean case from the NRL/NCSU model.

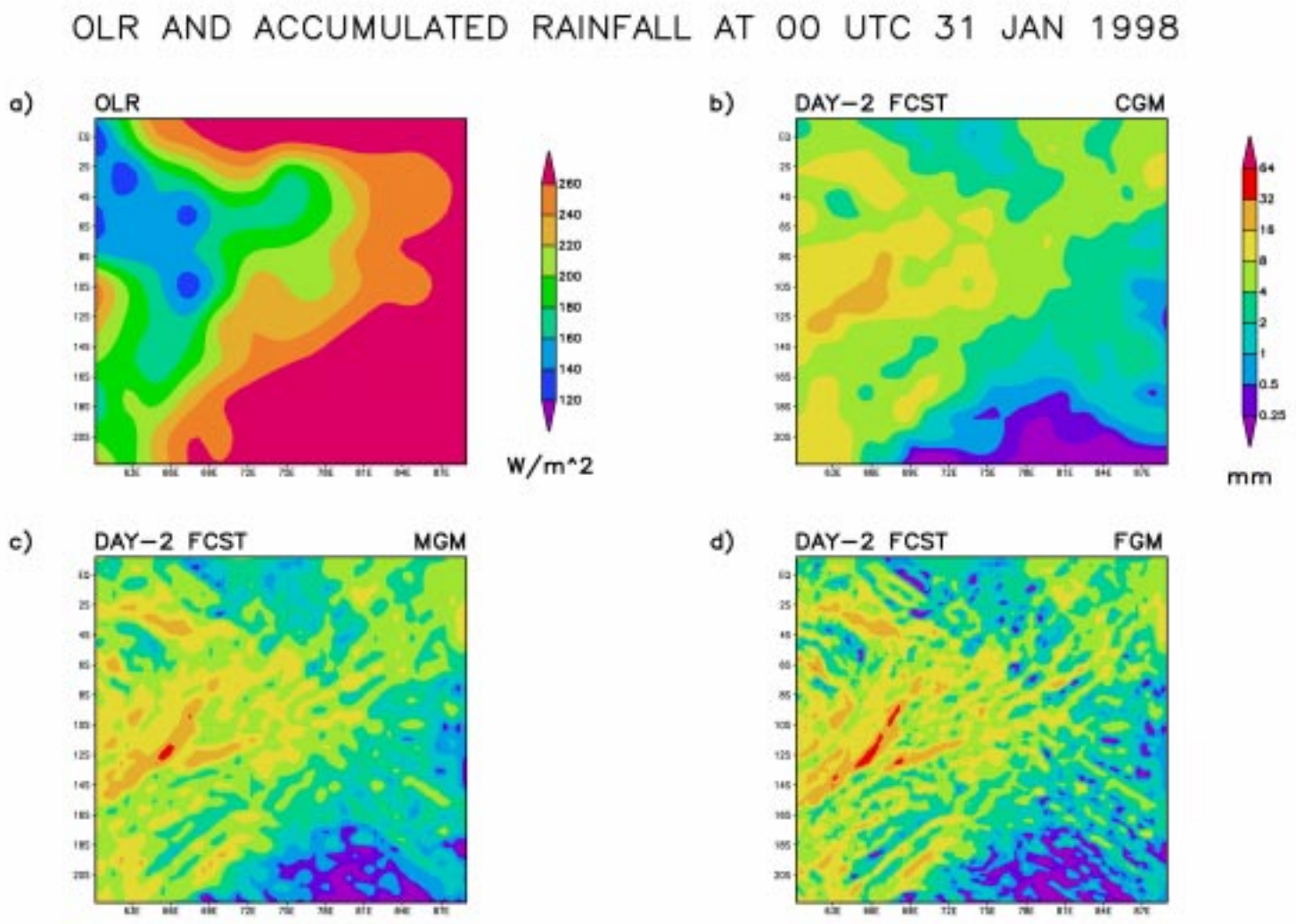

Figure 8.16. As in Fig. 8.15, except from the PSU-NCAR MM5.

Figures 8.17a-c show day-1 simulated mean meridional vertical velocity, specific humidity and temperature difference for 00 UTC 30 January 1997. The rising motions (negative vertical velocity) are found mainly in the eastern and western Indian Ocean (Fig. 8.17a). Compensating sinking motions (positive vertical velocity) are prevalent in the central Indian Ocean. The rising motions, particularly those in the eastern Indian Ocean, are in good agreement with the heavy rain areas, while sinking motions in the central Indian Ocean are consistent with no rain. The moistening (dry) regions particularly in the lower troposphere appear to be related with the rising (sinking) motions (Fig. 8.17b). The warmer atmosphere over the troposphere (Fig. 8.17c) is very pronounced. This suggests that advection by the mean flow and possible nonlinear effects may be important in maintaining large-scale temperature. At 00 UTC 31 January 1997, much stronger rising motions occur over the eastern Indian Ocean (not shown). The largest increase in water vapor is found to be due to the heaviest rainfall.

Figures 8.18a-c show day-1 simulated mean meridional vertical velocity, specific humidity and temperature differences for 00 UTC 30 January 1998. Weak rising motions are confined in the western Indian Ocean related with low rainfall rates. Strong sinking motions in the subsiding branch of the Walker circulation occur in the eastern Indian Ocean (Fig. 8.18a). Most interestingly, excess water vapor is generally located in the lower troposphere (Fig. 8.18b). The effect of increased SSTs during this ENSO event is to increase the water vapor contents in the lower troposphere. Due to the strong subsidence, the middle and upper troposphere are mostly dry. In contrast, the effect of warm SSTs is not reflected in a warming of the lower troposphere (Fig. 8.18c). The

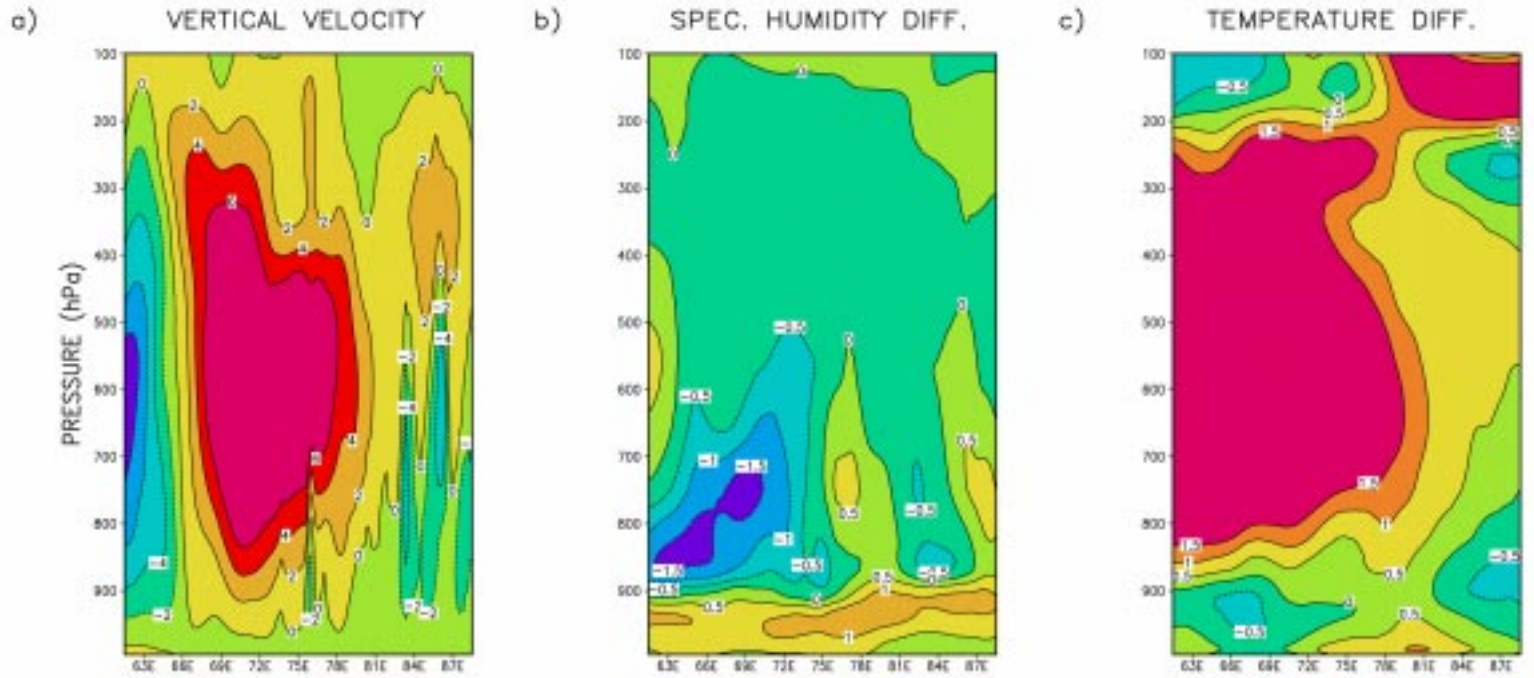

Figure 8.17. Zonal cross sections averaged between 0° and 15°S of day-1 a) simulated vertical velocity (mb/hr), b) specific humidity (g/kg) and c) temperature (K) differences between model simulation and analysis for 00 UTC 30 January 1997 for the Indian Ocean case from the NRL/NCSU model.

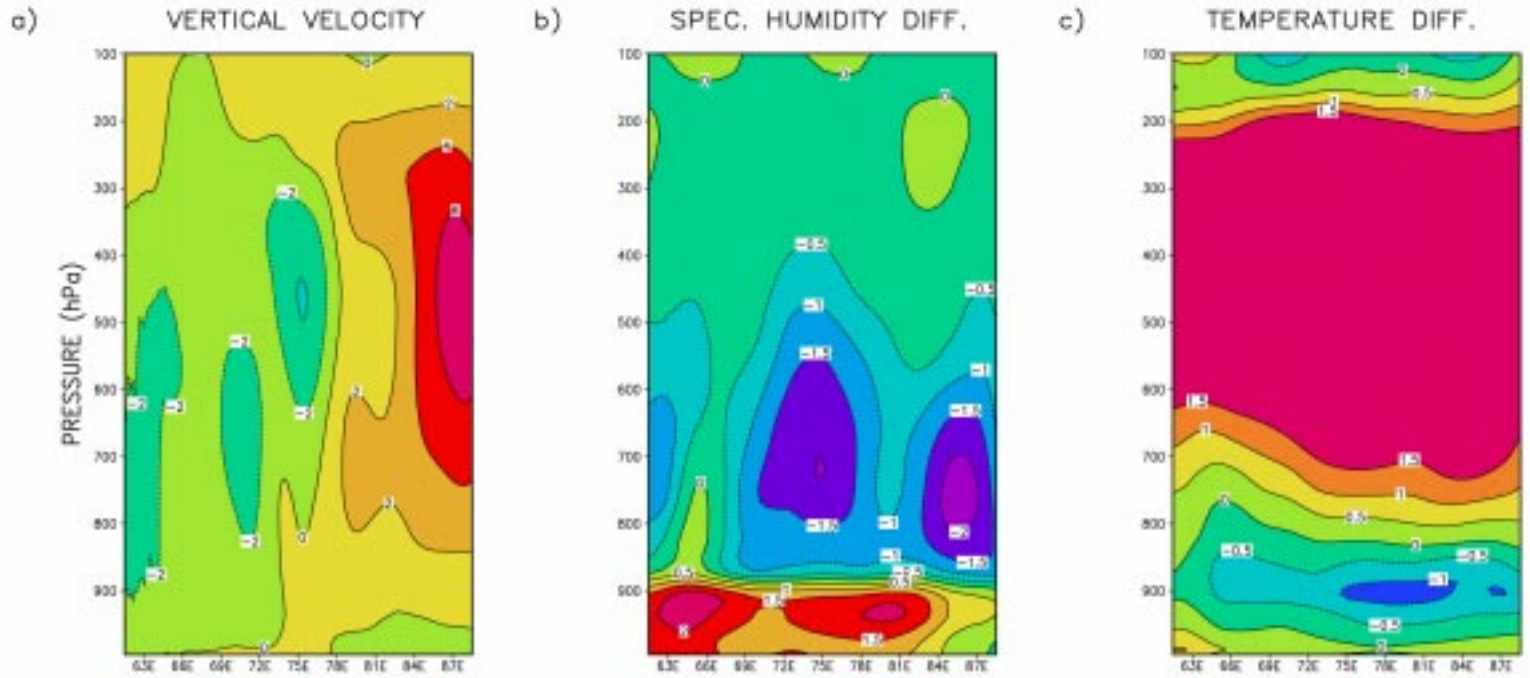

Figure 8.18. As in Fig. 8.17, except for 00 UTC 30 January 1998.

simulated lower troposphere is generally cool whereas the upper troposphere is warm. These features may be caused by the inability of the cumulus parameterization and the radiation schemes in maintaining the balance between dynamic and thermodynamic processes. The rising motions over the western Indian Ocean become strong at 00 UTC 30 January 1998 (not shown).

8.1.4 Spatial Distribution of Mean Kinetic Energy and Total Heat Flux

This section presents the spatial distributions of simulated daily mean kinetic energy and total surface heat flux (latent heat plus sensible heat) to investigate the effect of mesoscale circulations and SSTs on the rainfall distributions over the ITCZ region. The daily mean values are obtained by averaging values simulated every hour.

Figures 8.19a-b show day-1 simulated mean kinetic energy for 00 UTC 30 January 1997 and 00 UTC 30 January 1998, respectively. Strong gradients of kinetic energy (with amplitude 10-90 m^2s^{-2}) at 00 UTC 30 January 1997 corresponds to strong wind speed gradients along the band of the ITCZ (Fig. 8.19a). The generation of the kinetic energy gradients in this region is a manifestation of sharp contrasts in pressure difference between the subtropical high-pressure and the equatorial low-pressure systems.

During the ENSO event at 00 UTC 30 January 1998, gradients of kinetic energy do not exist in the Indian Ocean, except over a small area in the western Indian Ocean (Fig. 8.19b). An overall reduction of kinetic energy over the entire domain is also apparent. These results suggest that a uniform high-pressure system over the central-eastern Indian Ocean produces smaller wind speeds.

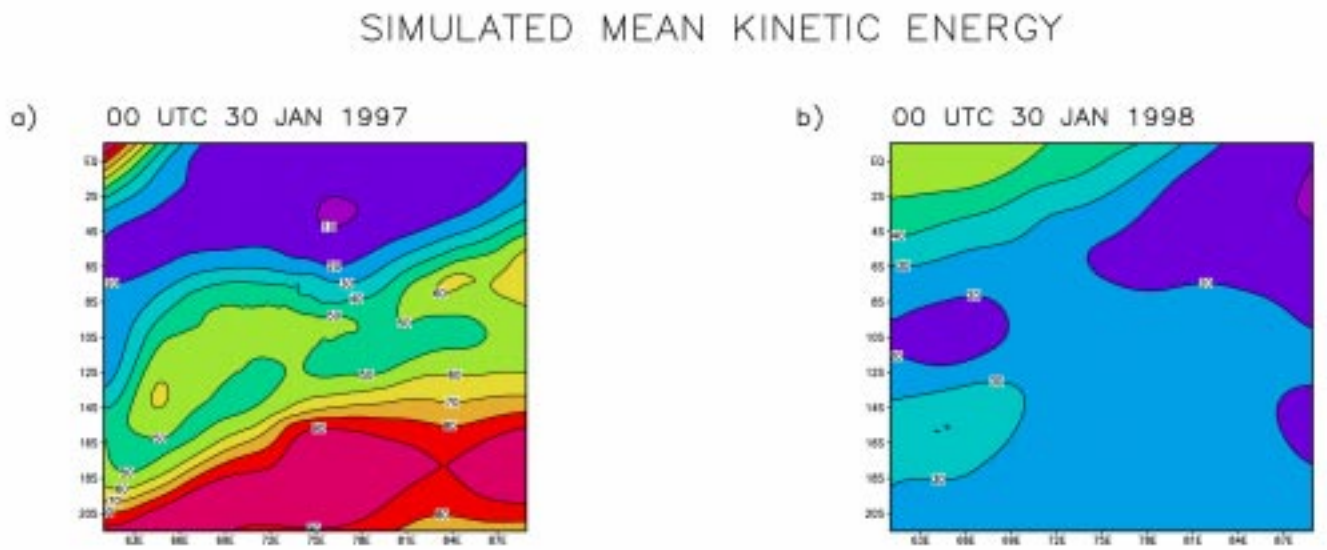

Figure 8.19. Distributions of day-1 simulated mean kinetic energy (m^2s^{-2}) for a) 00 UTC 30 January 1997 and b) 00 UTC 30 January 1998 for the Indian Ocean case from the NRL/NCSU model.

Figures 8.20a-b show day-1 simulated mean total surface heat flux for 00 UTC 30 January 1997 and 00 UTC 30 January 1998, respectively. There is general similarity between the spatial distributions of surface heat flux and that of kinetic energy for 00 UTC 30 January 1997. Strong surface heat flux gradients (with amplitude 100-200 Wm^{-2}) indicate large transport of moisture and heat from ocean to atmosphere. These gradients on either side of the ITCZ obviously play a key role in simulating strong convection and rainfall over the ITCZ.

In contrast, weaker surface heat flux gradients occur at 00 UTC 30 January 1998 (Fig. 8.20b). Moreover, the magnitudes of heat flux are relatively higher (maximum value = 280 Wm^{-2}) than those at 00 UTC 30 January 1997. It is obvious that direct response of local heating induced by increased SSTs during the ENSO event results in higher heat flux. However, lack of strong convergence and upward motions causes lower rainfall rates, particularly those over the eastern Indian Ocean.

8.1.5 Diurnal Variations of Rainfall, Vertical Velocity, and Total Heat Flux

This section presents hourly values of maximum rainfall, minimum vertical velocity, and maximum surface heat flux to investigate the diurnal variations during two contrasting oceanic environments.

Figures 8.21a-c show the maximum rainfall, minimum vertical velocity, and maximum heat flux as a function of Local Solar Time (LST) for 29 January to 31 January 1997. In general, distinct diurnal cycle of these variables is found during a typical northeast monsoon. Enhanced rainfall activity (minimum vertical velocity) is simulated in early morning hours with a maximum rate of 55 mm day^{-1} around 04 to 05 LST and

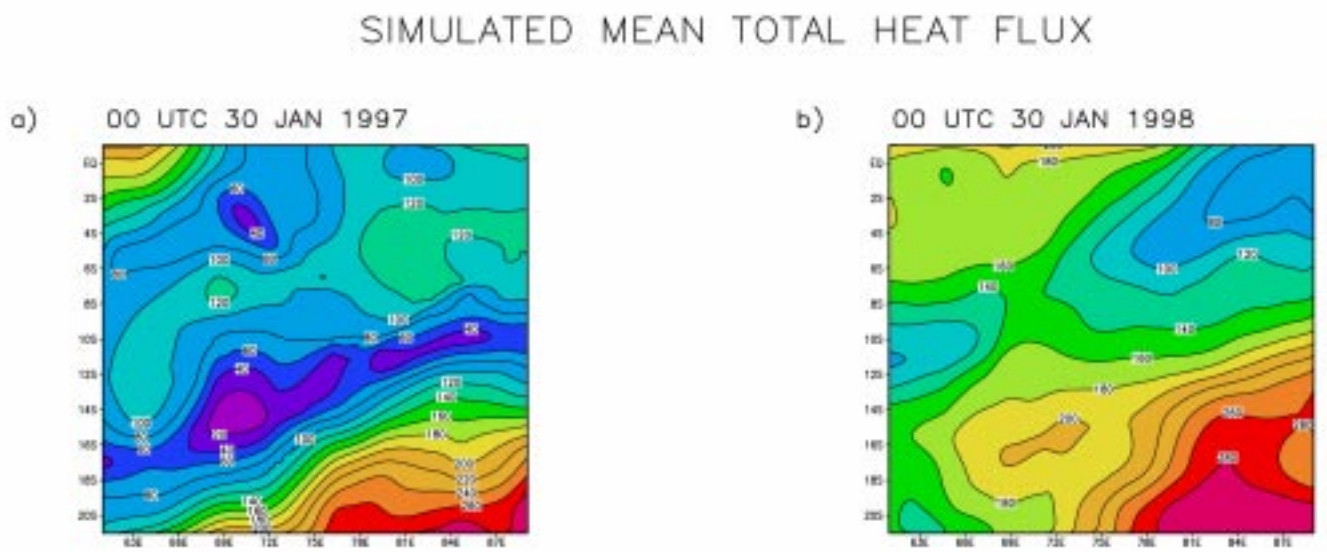

Figure 8.20. Distributions of day-1 simulated mean total heat flux (Wm^{-2}) for a) 00 UTC 30 January 1997 and b) 00 UTC 30 January 1998 for the Indian Ocean case from the NRL/NCSU model.

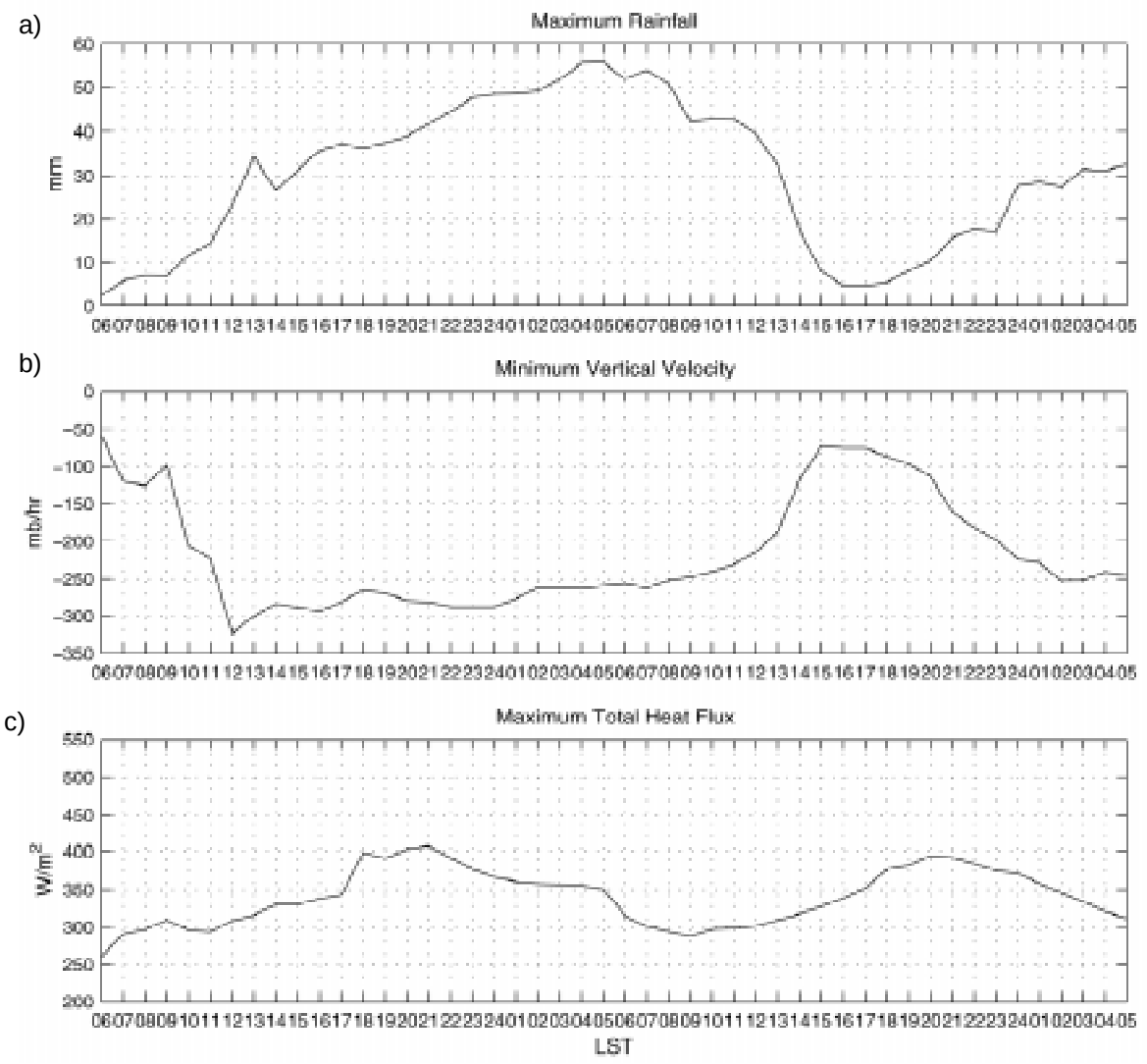

Figure 8.21. Diurnal variations of simulated a) maximum rainfall, b) minimum vertical velocity, and c) maximum total heat flux as a function of Local Solar Time (LST) for 29-31 January 1997 from the NRL/NCSU model.

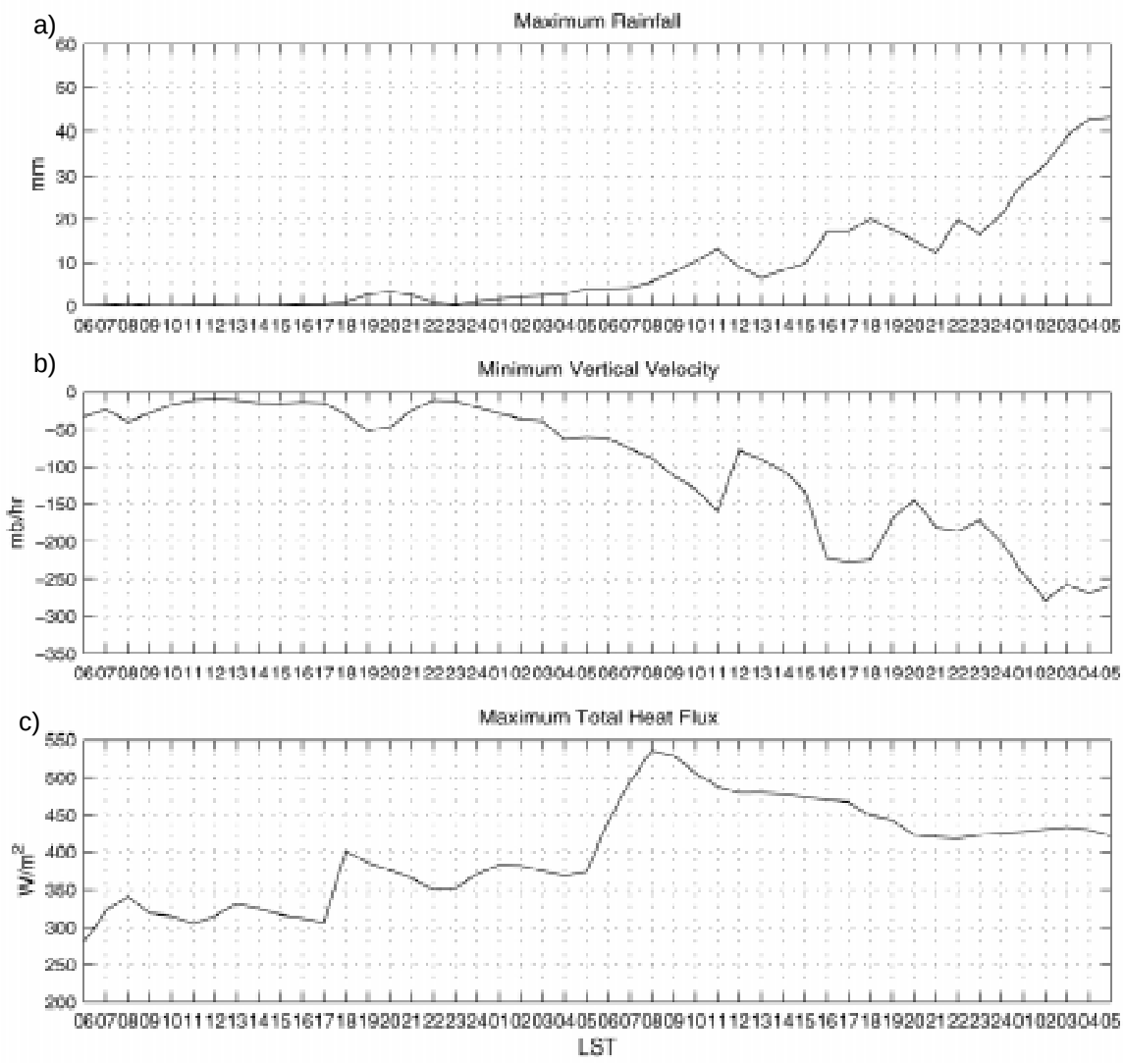

Figure 8.22. As in Fig. 8.21, except for 29-31 January 1998.